14-3-3γ affects dynamics and integrity of glial filaments by binding to phosphorylated GFAP

Huihui Li[1,2,3], Yan Guo[2], Junlin Teng[1,2], Mingxiao Ding[1,2], Albert Cheung Hoi Yu[4,5] and Jianguo Chen[1,2,3,*]

[1]The Key Laboratory of Cell Proliferation and Differentiation of Ministry of Education and The State Key Laboratory of Bio-membrane and Membrane Bio-engineering, [2]The Department of Cell Biology and Genetics, College of Life Sciences and [3]The Center for Theoretical Biology, Peking University, Beijing 100871, China
[4]Neuroscience Research Institute, Peking University, Beijing 100083, China
[5]Hong Kong DNA Chips Limited, Hong Kong SAR, China
*Author for correspondence (e-mail: chenjg@pku.edu.cn)

Summary

Recent findings indicated a protective role of GFAP in ischemic brain, injured spinal cord, and in neurodegenerative disease. We previously demonstrated that 14-3-3γ, once thought to be neuronal specific, was up-regulated by ischemia in astrocytes and may play a specific protective role in astrocytes. Here we report that 14-3-3γ associates with both soluble and filamentous GFAP in a phosphorylation- and cell-cycle-dependent manner in primary cultured astrocytes. The amount of association increases during G2/M phase due to more phosphorylated GFAP. Moreover, this interaction is independent of vimentin, another type III intermediate filament protein in astrocytes which forms glial filaments with GFAP. A series of domain deletion mutants and substitution mutations at phosphorylation sites (from serine to alanine) on GFAP demonstrated that serine 8 in the head domain is essential for the direct association of GFAP to 14-3-3γ. Overexpression of 14-3-3γ destroyed the integrity and affected the movement of GFAP intermediate filaments. This data demonstrates that 14-3-3γ contributes to the regulation of dynamics of GFAP filaments, which may contribute to the stability of the cytoskeleton and the mechanisms of central nervous system neurodegenerative disease.

Supplementary material available online at
http://jcs.biologists.org/cgi/content/full/119/21/4452/DC1

Key words: 14-3-3γ, GFAP, Vimentin, Astrocytes, Phosphorylation

Introduction

Intermediate filaments (IFs), the most complicated component of the cytoskeleton, are different from microtubules and microfilaments in several ways. First, there are six types and at least 65 kinds of known distinct IF proteins in human, expressed in a cell- and tissue-specific manner. They can homopolymerize or heteropolymerize into 10 nm diameter filaments. Second, all IF proteins have the same secondary structure molecular motifs, consisting of a globular head domain, an alpha-helical rod domain and a carboxyl-terminal tail domain. Mutations in different IFs result in human genetic diseases including neurodegeneration, premature ageing, severe tissue fragility and myopathies (Magin et al., 2004). Despite that there are numerous studies on the dynamics, function and structure of IFs, based on their importance in human health, much still remains to be understood.

Glial fibrillary acidic protein (GFAP) is a type III IF protein and a marker of astrocytes, the most abundant cell type in the mammalian central nervous system (CNS). GFAP assembles with vimentin to form glial filaments, which stabilize astrocytic processes (Weinstein et al., 1991; Wilhelmsson et al., 2004). Previous research showed that glial filaments are involved in many roles of astrocytes, such as the long-term maintenance of brain architecture, the proper functioning of the blood-brain

barrier, and the modulation of some neuronal functions (Liedtke et al., 1996). In human, GFAP mutations cause Alexander disease, a progressive neuropathy accompanied by astrocyte degeneration (Brenner et al., 2001). The expression level of GFAP is significantly increased in reactive astrocytes, also suggesting that it has important roles in CNS ischemia, trauma, tumors, and in many neurodegenerative conditions (Pekny and Nilsson, 2005). In certain phases of the cell cycle, GFAP can be phosphorylated by specific kinases, which has been shown to regulate GFAP filament assembly (Matsuoka et al., 1992). However, the mechanisms of GFAP regulation require further elucidation.

14-3-3 proteins, originally isolated as abundant, cytosolic, rabbit brain proteins (Moore and Perez, 1967), exist as a family of several highly similar yet distinct protein isoforms from seven genes (assigned β, ε, γ, η, σ, τ and ζ). The striking feature of 14-3-3 proteins is their ability to bind a multitude of functionally diverse signaling proteins, including kinases, phosphatases and transmembrane receptors (Dougherty and Morrison, 2004). The ability of 14-3-3 to bind target proteins depends on the phosphorylation of specific sites in the target proteins (Dougherty and Morrison, 2004; Yaffe and Elia, 2001). In epithelial cells, 14-3-3ζ proteins bind to phosphorylated keratin 18, a type I IF protein, during the cell cycle, and act as solubility cofactors to modulate keratin

filaments and hepatocyte mitotic progression (Ku et al., 1998; Ku et al., 2002; Liao and Omary, 1996). It is known that 14-3-3 proteins play important roles in modulating the structure of IFs, cell mitotic progression, apoptosis, and in multiple signal transduction pathways by acting as scaffolds for, and regulators of, signaling proteins (Fu et al., 2000; Hermeking, 2003).

Among the members of 14-3-3 protein family, the γ isoform was thought to be brain- and neuron-specific (Watanabe et al., 1993). Though now seven isoforms of 14-3-3 protein can all be detected in the astrocytes (Satoh et al., 2004), our previous data demonstrated that 14-3-3γ was specifically up-regulated by in vitro ischemia in primary cultures of astrocytes (Chen et al., 2003). 14-3-3γ and GFAP are now both known to play protective roles in reactive astrocytes under ischemia and in neurodegenerative diseases (Chen et al., 2003; Fountoulakis et al., 1999; Pekny and Nilsson, 2005), therefore we were interested in elucidating whether 14-3-3γ and GFAP interact in astrocytes. Results demonstrated that 14-3-3γ associated with phosphorylated GFAP in both soluble and insoluble forms, but independently of the interaction between 14-3-3γ and vimentin, a non-astrocyte specific IF protein.

Results

Association of 14-3-3γ and GFAP in astrocytes

Coimmunoprecipitation was used to determine whether endogenous 14-3-3γ and GFAP physically interact. Immunoprecipitation of GFAP proteins from the NP-40 lysate of astrocytes resulted in a co-precipitation of 14-3-3γ (Fig. 1A, bottom, lane 3). Interestingly, another isoform, 14-3-3η could not be detected in GFAP immunoisolated complexes (supplementary material Fig. S1). Western blot analysis demonstrated the existence of vimentin with GFAP and 14-3-3γ in the NP-40 soluble fraction of cultured astrocytes (Fig. 1A, lane 1). Vimentin was also precipitated with GFAP from the NP-40 soluble fraction (Fig. 1A, top, lane 3). In addition, vimentin and 14-3-3γ were detected in the post-NP-40 pellet (Fig. 1A, lane 4). At the same time, immunoprecipitation of vimentin proteins also resulted in a coimmunoisolation of GFAP and 14-3-3γ (Fig. 1B).

Interaction of 14-3-3γ, GFAP and vimentin in SW13 cells

As astrocytes express both GFAP and vimentin, which co-assemble to form 10 nm filaments, an absence of endogenous IFs would provide an ideal model for studying single IF proteins. To study whether vimentin is necessary for the association of GFAP and 14-3-3γ, we chose vimentin (–) SW13 Cl2 cells, in which no endogenous IFs are expressed (Fig. 1C) (Chen and Liem, 1994; Sarria et al., 1990). To detect the interaction between GFAP and 14-3-3γ in the absence of vimentin, GFAP was transfected into SW13 Cl2 cells (Fig. 1E). Endogenous 14-3-3γ was immunoprecipitated by rabbit anti-GFAP polyclonal antibody (Fig. 1F, bottom, lane 3), and the results of western blot showed that the detergent insoluble fraction also contained 14-3-3γ in Cl2 cells. Thus, the interaction between GFAP and 14-3-3γ was independent of vimentin. In addition, to study whether there exists any interaction between 14-3-3γ and vimentin, we chose vimentin (+) SW13 Cl1 cells, in which vimentin is the only kind of IF protein expressed (Fig. 1C) (Chen and Liem,
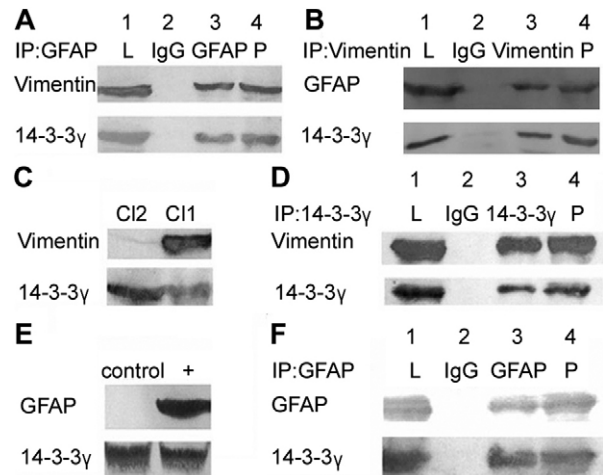

Fig. 1. Association of 14-3-3γ and GFAP is independent of vimentin. (A) Immunoprecipitation assay by GFAP antibody in astrocytes. The astrocyte extracts (lane 1) were subjected to immunoprecipitation with a rabbit preimmune IgG (lane 2) or a rabbit anti-GFAP antibody (lane 3) and subsequent western blot analysis with mouse anti-vimentin antibody (top) or mouse anti-14-3-3γ antibody (bottom). The pellet was also detected by vimentin and 14-3-3γ antibodies (lane 4). (B) Immunoprecipitation assay by vimentin antibody in astrocytes. The astrocyte extracts (lane 1) were subjected to immunoprecipitation with a mus preimmune IgG (lane 2) or a mus anti-vimentin antibody (lane 3) and subsequent western blot analysis with rabbit anti-GFAP antibody (top) or mouse anti-14-3-3γ antibody (bottom). The pellet was also detected by GFAP and 14-3-3γ antibodies (lane 4). (C) Western blot analysis of SW13 Cl1 (lane Cl1) and SW13 Cl2 (lane Cl2) using specific antibodies to vimentin (top) and 14-3-3γ (bottom). (D) Immunoprecipitation of 14-3-3γ and vimentin. The extracts of SW13 Cl1 cells (lane 1) were subjected to immunoprecipitation with a rabbit preimmune IgG (lane 2) or the rabbit anti-14-3-3γ antibody (lane 3) and subsequently detected with mouse anti-vimentin antibody (top) or mouse anti-14-3-3γ antibody (bottom). The pellet was also subjected to western blot (lane 4). (E) Results of western blot of pcDNA3.1-GFAP transfected SW13 Cl2 cells. The proteins were detected by mouse anti-GFAP antibody (top) or mouse anti-14-3-3γ antibody (bottom). The same amount of untransfected cells was used as in control (lane control). (F) The interaction of GFAP and 14-3-3γ in pcDNA3.1-GFAP transfected SW13 Cl2 cells. SW13 Cl2 extracts transiently expressing GFAP (lane 1) were subjected to immunoprecipitation with rabbit anti-GFAP antibody (lane 3) or a rabbit preimmune IgG (lane 2) and subsequent western blot with mouse anti-GFAP antibody (top) or mouse anti-14-3-3γ antibody (bottom). The pellet was also subjected to western blot analysis (lane 4).

1994; Sarria et al., 1990). An immunoprecipitation assay was performed in SW13 Cl1 cells using rabbit anti-14-3-3γ polyclonal antibody and results showed that vimentin existed in the immunoprecipitated complex (Fig. 1D, top, lane 3). The result of western blot analysis showed that both 14-3-3γ and vimentin also existed in NP-40 insoluble components (Fig. 1D, lane 4). Thus, the interaction of vimentin and 14-3-3γ is independent of GFAP. In this study, endogenous expression of 14-3-3γ was confirmed in SW13 Cl1 and Cl2 cell lines (Fig. 1C).

Association of 14-3-3γ and GFAP under phosphorylation and dephosphorylation treatment

To examine the effect of phosphorylation of GFAP on its binding to 14-3-3γ, we use Calyculin A (Cl-A), a potent and specific inhibitor of type 1 (PP1) and type 2A (PP2A) serine/threonine phosphatases, for hyperphosphorylation treatment, and calf intestine alkaline phosphatase (CIAP) for dephosphorylation treatment. In the immunoprecipitation assay, the phosphorylated GFAP still associated with 14-3-3γ after Calyculin A-treatment (Fig. 2A, lane 1). By contrast, the interaction between GFAP and 14-3-3γ could not be detected after dephosphorylation treatment by CIAP (Fig. 2A, lane 4). Interestingly, the incubation of the cell lysate first with Calyculin A and then with CIAP prevented GFAP binding to 14-3-3γ (Fig. 2A, lane 3). Similar results were obtained in primary cultured astrocytes (data not shown). Thus, the association of GFAP with 14-3-3γ still exists under the hyperphosphorylation of GFAP, while dephosphorylation of GFAP completely prevents its binding to 14-3-3γ. The hyperphosphorylation and dephosphorylation treatments showed similar effects on the association between vimentin and 14-3-3γ (supplementary material Fig. S2).

We then went on to detect the change in association between GFAP and 14-3-3γ by cdc2 kinase or PKC, which have been found to phosphorylate GFAP at specific sites (Matsuoka et al., 1992; Yasui et al., 1998). GFAP in the cell lysate was immunoisolated by antibody and beads. After CIAP and cdc2 kinase or PKC treatment, beads with the immunoisolated GFAP were incubated with cell lysates again. The results showed that the association of GFAP and 14-3-3γ was increased obviously after cdc2 kinase or PKC treatment (Fig. 2B, lanes 2 and 3), which supports the observation that this interaction is regulated by phosphorylation.

Association of GFAP and 14-3-3γ during the cell cycle

It has been shown that phosphorylation is a principal factor in the regulation of IF assembly, disassembly and subcellular organization. Hyperphosphorylation of IFs is directly correlated with their disassembly into non-filamentous soluble structures (Kawajiri et al., 2003). Under physiological conditions, it is known that GFAP becomes hyperphosphorylated during S and G2/M phases of the cell cycle (Sekimata et al., 1996). To elucidate whether the change in GFAP phosphorylation during the cell cycle would affect its interaction with 14-3-3γ, we synchronized astrocytes in primary cultures at G1/S stages of the cell cycle by aphidicolin treatment (Liao and Omary, 1996), and carried out coimmunoprecipitation assays. Results showed a significant increase in the association of 14-3-3γ with GFAP 6 hours after release of the cycle block (Fig. 3A, lane 2 and 3), when most astrocytes were likely to be in S phase. This association remained at a similar level after 12 hours when most astrocytes appeared to be entering G2/M phases. The binding decreased at 18 hours (Fig. 3A, lane 4) when most cells have usually left M phase and entered G1 phase, but increased again at 22 hours for recycling to S phase (Fig. 3A, lane 5) (Liao and Omary, 1996). The increase in the association coincident with the timing of S and G2/M phases of the cell cycle, also correlated with IFs hyperphosphorylation (Liao and Omary, 1996; Sekimata et al., 1996). This lends support to our observations with
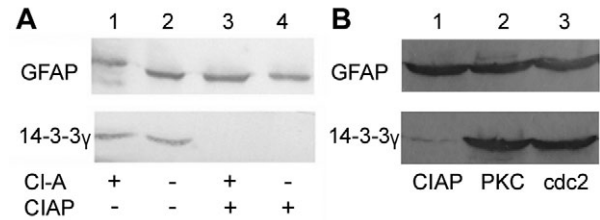

Fig. 2. Effect of the hyperphosphorylation of GFAP on the association of GFAP and 14-3-3γ. (A) GFAP immunoprecipitation from GFAP transfected SW13 Cl2 cells by hyperphosphorylation and dephosphorylation treatments. The cells were treated with serum-deprived medium (lanes 2 and 4) or medium containing 100 nM Calyculin A (lanes 1 and 3). Then the cell lysate was incubated with buffer alone (lanes 1 and 2) or with CIAP (lanes 3 and 4). The immunoprecipitates were blotted with anti-GFAP or anti-14-3-3γ antibody. (B) GFAP immunoprecipitation from GFAP transfected SW13 Cl2 cells by kinase treatments. The cell lysate was incubated with beads and GFAP antibody. After centrifugation, GFAP binding complex was incubated with CIAP for 30 minutes and then, was treated with cdc2 kinase (lane 2) or PKC (lane 3) in relative buffer. Then fresh cell lysate was incubated with kinase treated GFAP binding complex and the final immunoprecipitates were blotted with anti-GFAP or anti-14-3-3γ antibody.

Calyculin A-treated cultures, suggesting that the binding of 14-3-3γ to GFAP is GFAP phosphorylation-dependent.

Using triple fluorescence staining, we confirmed that the association of 14-3-3γ with GFAP in astrocytes changed with cell cycle progression. The colocalization of 14-3-3γ and GFAP in the stage of cytokinesis at the end of mitosis displayed a punctate pattern in the cytoplasm, and some 14-3-3γ not colocalized with GFAP was observed at the area of the contractile ring (Fig. 3Ba-c). In interphase, the distribution of GFAP and 14-3-3γ existed in three patterns. In most cells, soluble GFAP in mitosis completely assembled into filamentous structures, and punctate 14-3-3γ showed no colocalization with filamentous GFAP. In some cells, 14-3-3γ remained in a punctate distribution and seemed to only associate with non-filamentous GFAP (Fig. 3Bd-f). In only a few interphase cells, did 14-3-3γ show some colocalization with both soluble and filamentous GFAP (data not shown). When astrocytes entered prophase of mitosis, the fluorescent images revealed that 14-3-3γ proteins were bound to most filamentous GFAP before GFAP filament disassembly (Fig. 3Bg-i). However, when GFAP filaments were disassembled, 14-3-3γ bound to more soluble GFAP (Fig. 3Bj-l). Thus, 14-3-3γ binding to soluble GFAP occurred at all phases of the cell cycle, and its colocalization with filamentous GFAP was observed in many prophase cells before filament disassembly but in only a few interphase cells. From these data demonstrating changes in 14-3-3γ and GFAP colocalization during the cell cycleobserved after astrocyte synchronization (Fig. 3), we concluded that the association we detected by immunoprecipitation may be cell cycle-regulated.

Domain mapping of GFAP in the interaction with 14-3-3γ

GFAP (429 amino acid residues) contains an N-terminal head domain (1–69), an α-helix rod domain (70-374) and a C-terminal tail domain (375–429). Most GFAP phosphorylation
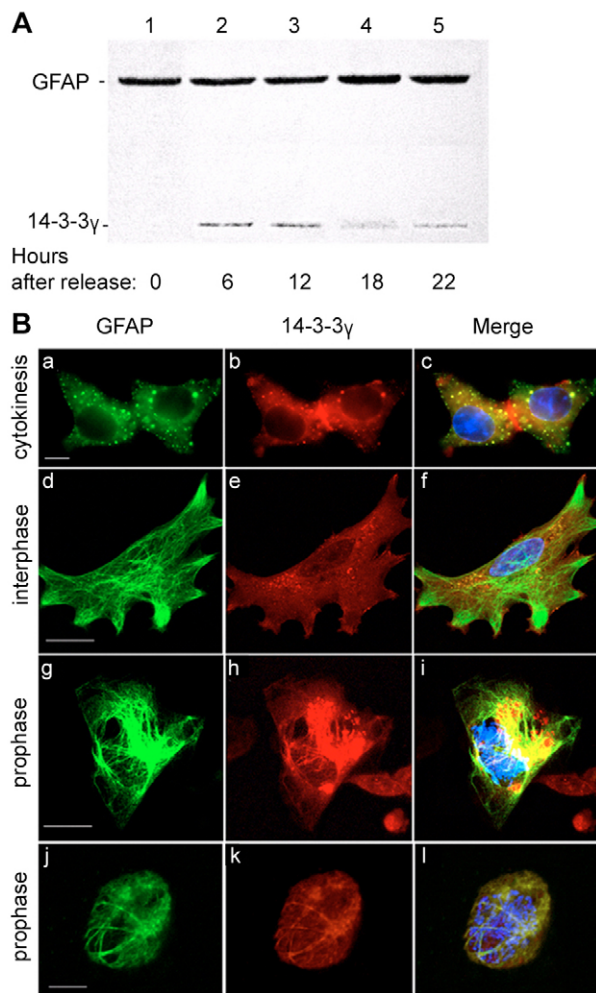
Fig. 3. Association of 14-3-3γ with GFAP during the cell cycle. (A) Coimmunoprecipitation of GFAP and 14-3-3γ in synchronized astrocytes using GFAP antibody. The primary astrocytes were blocked at G1/S phase using aphidicolin (lane 1). Then the cells were released from the block for the indicated time (lanes 2-5). (B) Immunofluorescent triple staining of astrocytes in different phases of the cell cycle with GFAP (green), 14-3-3γ (red) and DNA (blue). Scale bars, 10 μm.

is found in the head and tail domains. To dissect the domain of GFAP involved in the association with 14-3-3γ, head and tail domain deletion mutants (ΔH and ΔT) with a C-terminal c-myc tag expression vector were constructed (Fig. 4A). The normal expression of transfected GFAP, domain deletion mutants and endogenous 14-3-3γ in SW13 Cl2 cells was confirmed by western blot (Fig. 4B). After introducing these vectors into Cl2 cells, immunoprecipitation assays were performed with c-myc antibody. 14-3-3γ was coimmunoprecipitated by GFAP or ΔT-GFAP in vivo, demonstrating that these still possessed the 14-3-3γ interaction domains, while 14-3-3γ could not be detected in ΔH-GFAP immunoprecipitated complexes (Fig. 4B). These results indicate that the head domain of GFAP is essential for its association with 14-3-3γ. This notion was further supported by

immunostaining experiments in SW13 Cl2 cells. Fluorescence micrograph showed that c-myc tagged GFAP can assemble into filamentous structures by themselves. In a few Cl2 cells, endogenous 14-3-3γ colocalized with GFAP filaments and dots (Fig. 4Ca-c). Neither of the deletion mutants, ΔH-GFAP nor ΔT-GFAP, could form filamentous structures and they both showed a diffuse or dot-like distribution in the cytoplasm. 14-3-3γ was colocalized with ΔT-GFAP punctate form (Fig. 4Cg-i), while 14-3-3γ and ΔH-GFAP showed no colocalization (Fig. 4Cd-f).

FRET assay can detect the direct interaction between two proteins tagged with fluorescence proteins in vivo. When two proteins are within a distance of 10 nm, the fluorescent tags can cause the FRET effect. This can be detected by confocal microscopy, and its efficiency, indicating the likelihood of direct protein interaction, can be calculated by Leica SPII FRET software. Here we used bleaching treatment and FRET assay to detect whether the interaction between 14-3-3γ and GFAP or the GFAP deletion mutants was direct. We constructed a donor vector with CFP tagged 14-3-3γ and three acceptor vectors with YFP tagged GFAP or GFAP domain deletion mutants. Donor and acceptor vectors were transfected into SW13 Cl2 cells together. When the fluorescence of the acceptor (GFAP-YFP) was bleached, the intensity of the donor (14-3-3γ-CFP) fluorescence increased compared with the value before bleaching (Fig. 4D, red arrow and Fig. 4E, ROI1). GFAP-YFP and 14-3-3γ-CFP showed about 21% higher FRET efficiency (Ef) than the control efficiency (Cf) about 1% in the unbleached zone (Fig. 4D, white arrow, Fig. 4E, ROI2 and Fig. 4F). Although GFAP-YFP could not assemble into filaments in endogenous IF-absent cells, as could GFAP-c-myc, this did not affect the FRET measurements. By contrast, the FRET efficiency of ΔH-GFAP-YFP and 14-3-3γ-CFP was not different from that of the control (Cf). On average, FRET efficiency between 14-3-3γ-CFP and GFAP-YFP or ΔT-GFAP-YFP was higher than that of 14-3-3γ-CFP and ΔH-GFAP-YFP (Fig. 4F). This demonstrated that GFAP and ΔT-GFAP can interact with 14-3-3γ directly in vivo. By contrast, ΔH-GFAP cannot interact with 14-3-3γ, consistent with the results obtained using coimmunoprecipitation and immunostaining (Fig. 4B,C).

Functional phosphorylation site of GFAP needed for interaction with 14-3-3γ

Four different possible serine phosphorylation sites exist in the head domain of mouse GFAP (Fig. 5A) (Yasui et al., 1998). We made four site mutants (S8A, S12A, S15A and S35A, substituting serine with alanine) tagged with c-myc to determine which phosphorylation site on GFAP was essential in the association with 14-3-3γ (Fig. 5A). The results of immunofluorescence by c-myc antibody showed that all of these four site mutants could self-assemble into filaments in transfected SW13 Cl2 cells (Fig. 5Ba,d,g,j). 14-3-3γ and GFAP did not show colocalization in most S8A GFAP transfected cells (Fig. 5Ba-c), however, in some cells transfected with the other three mutants, 14-3-3γ colocalized with filamentous GFAP (Fig. 5Bd-l). Quantification of the colocalization of GFAP mutants and 14-3-3γ in interphase cells also showed that GFAP S8A mutant hardly colocalized with 14-3-3γ, while some colocalization was observed for punctuate or filamentous forms in nearly 10-15% of cells for
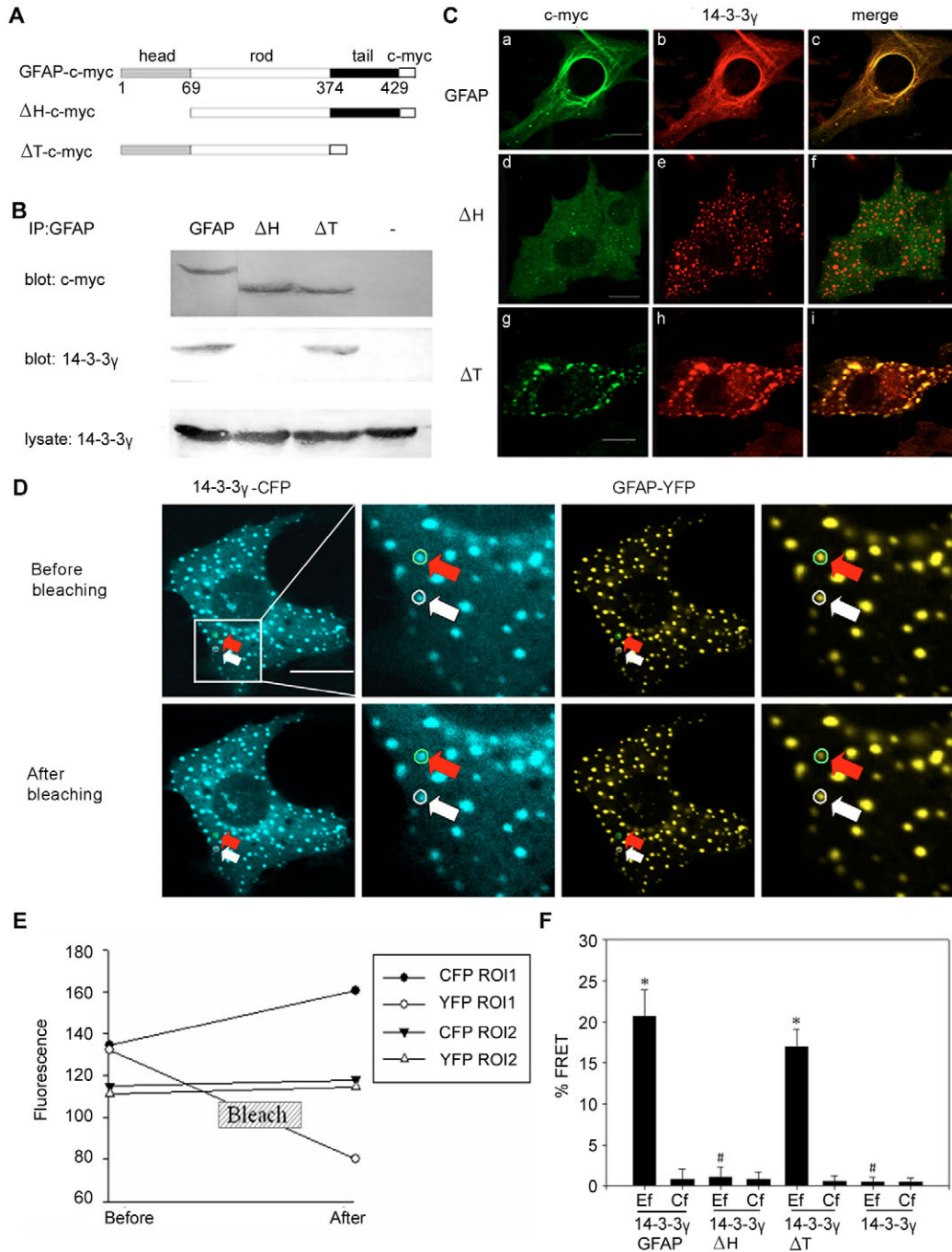
Fig. 4. Identification of the 14-3-3γ interaction domain of GFAP. (A) Schematic presentation of GFAP and its deletion mutants. Like all IF proteins, GFAP contains an N-terminal head domain, a C-terminal tail domain and a conserved α-helical rod domain. Two deletion mutants (ΔH and ΔT) of GFAP were constructed by PCR, and c-myc was inserted into the C-terminal of the mutants. (B) The immunoprecipitation assay of c-myc tagged GFAP and its deletion mutants with 14-3-3γ. SW13 Cl2 cell extracts were subjected to immunoprecipitation with rabbit anti-GFAP antibody, subsequent western blot with the mouse anti-c-myc (upper) and anti-14-3-3γ (middle) antibodies. Whole cell lysates were also subjected to western blot by 14-3-3γ antibody as the control (bottom). (C) Colocalization of GFAP and 14-3-3γ. SW13 Cl2 cells were transfected with GFAP and its mutants (ΔH and ΔT). The cells were immunostained by mouse anti-c-myc antibody (green) and rabbit anti-14-3-3γ antibody (red). (D) FRET between 14-3-3γ-CFP and GFAP-YFP in transfected SW13 Cl2 cells. The fluorescent images showed the recordings immediately before and after the photobleaching cycle. The bleaching zone (ROI1) was marked with a red arrow and the control zone (ROI2) was marked with a white arrow. (E) The plot shows the fluorescence intensities in the two regions for each channel in Fig. 4D. (F) FRET efficiencies (Ef) between 14-3-3γ-CFP and YFP-tagged GFAP deletion mutants. Ef is represented as the differences of CFP fluorescence before and after YFP photobleaching in defined regions (ROI 1, see Fig. 4D). Similar calculations were done in a non-bleached region (ROI 2) of comparable intensity of the same cell to calculate the control value (Cf). In each experiment, n=10 cells were recorded and analyzed per condition. *The differences between the paired Ef and Cf values marked by asterisks are highly significant ($P<0.001$). The differences between the paired Ef and Cf values marked by # were not significant ($P>0.05$). Scale bar, 10 μm. Scale bar in magnified figure, 5 μm.
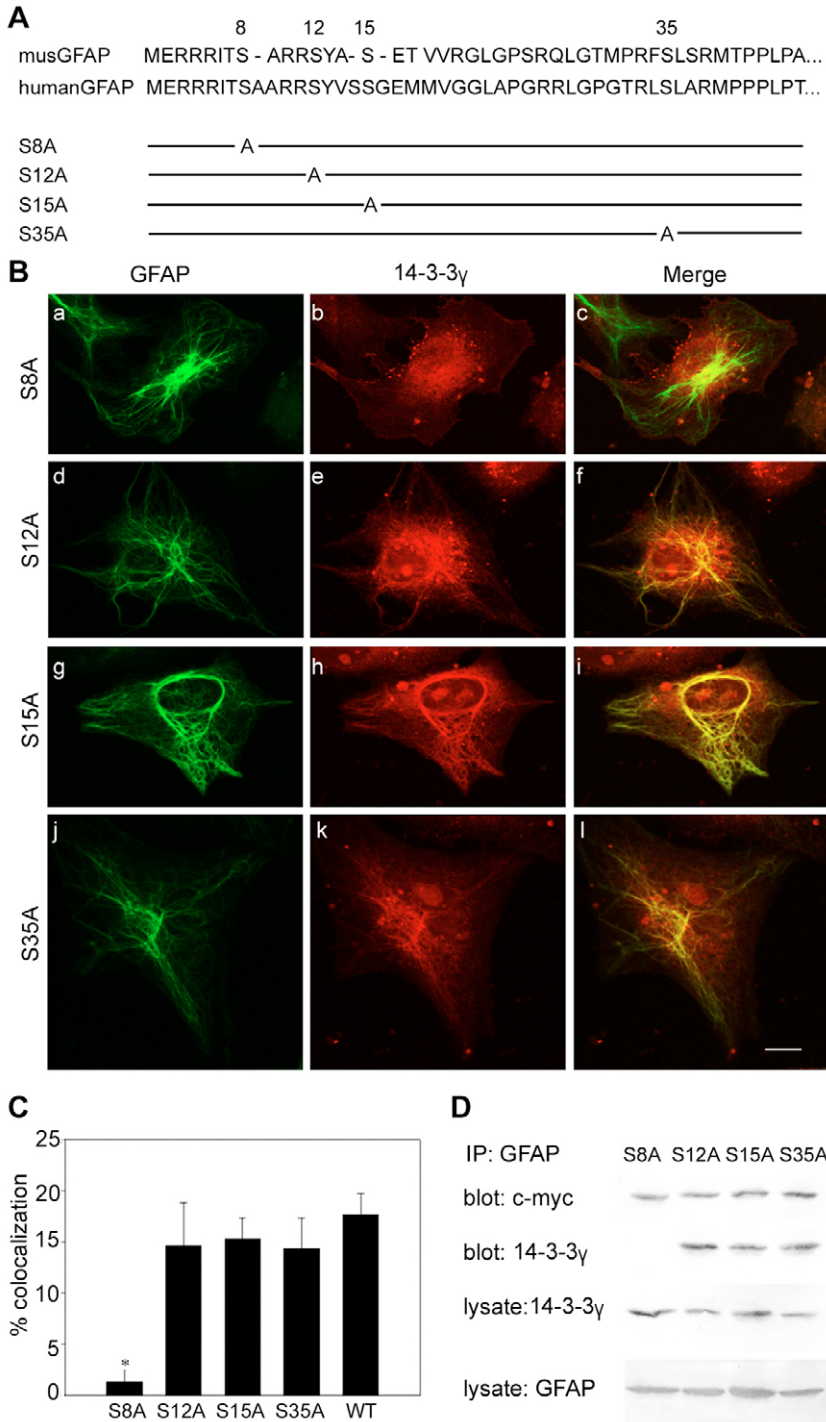
Fig. 5. Requirement of GFAP phosphorylation at Ser8 for GFAP-14-3-3γ interaction. (A) Schemes showing the N-terminal amino acid sequences of human and mouse GFAP (upper), and its substitution mutations (below). (B) Representative immunostaining images of GFAP mutants and 14-3-3γ in transfected SW13 Cl2 cells. Scale bar, 10 μm. (C) The bar graphs show quantification of the colocalization of GFAP mutants and 14-3-3γ in (B). In each experiment, transfected interphase cells (*n*=100) were recorded and the displayed data are representative of three independent experiments. *The differences between S8A and WT (wide type) values marked by asterisks are highly significant (*P*<0.001). The differences between other mutants and WT values showed no significance (*P*>0.05). (D) The immunoprecipitation assay of GFAP and its serine site mutants with 14-3-3γ. Extracts from mutant transfected SW13 Cl2 cells were subjected to immunoprecipitation with rabbit anti-GFAP antibody, and subsequent western blot with mouse anti-14-3-3γ and anti-c-myc antibodies. Whole cell lysates were also detected by mouse 14-3-3γ antibody and rabbit GFAP antibody as the control.

the other three mutants (Fig. 5C). The phase in cell cycle was identified by the shape of the nucleus stained with Hoechst 33342 (figure not shown). This indicated an important role for GFAP serine 8 in the GFAP-14-3-3γ association. Coimmunoprecipitation experiments in transfected SW13 Cl2 cells further confirmed this finding. Antibodies against GFAP could immunoisolate 14-3-3γ from all mutant GFAP transfected cells except from cells transfected with S8A GFAP (Fig. 5D). This proved that GFAP serine 8 is necessary for GFAP binding to 14-3-3γ.

Assembly and movement of GFAP by overexpression of 14-3-3γ

14-3-3 family proteins play an important role in the regulation of the activities of their target proteins and it is known that the expression of 14-3-3 is increased in neurodegenerative disease (Fountoulakis et al., 1999; Van Everbroeck et al., 2005). To investigate the regulatory function of 14-3-3γ proteins in GFAP activity through their interaction in gliomas or reactive astrocytes, we overexpressed 14-3-3γ in rat glioma C6 cells, and observed the GFAP filaments. In most untransfected or

control vector, pDsRed-N1, transfected cells, endogenous GFAP showed a regular filament-like distribution (Fig. 6Aa-c). In most DsRed-14-3-3γ transfected cells, endogenous GFAP showed both dots and filamentous structures (Fig. 6Ad-f). In some cells, DsRed-14-3-3γ induced the formation of GFAP aggregation and the disassembly of filamentous GFAP, causing the GFAP filamentous network to be completely disrupted and to appear as an aggregation of dots (Fig. 6Ag-i). These results were quantified in Fig. 6B and clearly demonstrate that high concentrations of exogenous 14-3-3γ facilitate the disassembly of most GFAP filaments. During mitosis, GFAP filaments can be disassembled into dots without exogenous overexpression of 14-3-3, so, to confirm all the observed cells were in interphase, we detected the nuclear shape by Hoechst 33342 staining.

We also downregulated the expression of 14-3-3γ in C6 cells by RNA interference to study the regulatory role of 14-3-3γ in

Fig. 6. Phenotype of glial filaments by overexpression of 14-3-3γ. (A) C6 cells were transfected with DsRed-14-3-3γ or DsRed, and GFAP filaments were visualized by immunostaining with GFAP antibody. (a) Normal glia filaments immunostained with rabbit GFAP antibody. (b-c) pDsRed-N1 vector transfection (c, red) did not affect GFAP filaments (b). (d-i) In DsRed-14-3-3γ overexpressing cells (e,h), endogenous GFAP (d,i) showed an aggregation of dots. Scale bar, 10 μm. (B) Distribution of glial filaments in the population of cells expressing the indicated proteins. A minimum of 100 cells was randomly scored in a blinded manner. Each transfection was repeated three times with similar results.

glial filament assembly. As shown in supplementary material Fig. S3A, a significant loss of 14-3-3γ expression was detected by immunoblotting analysis after cells had been transfected with plasmid coding for 14-3-3γ siRNA. At the same time, the levels of GFAP and actin were not changed after 14-3-3γ siRNA transfection. The distribution of glial filaments in the population of cells transfected with different plasmids was quantified. We detected no distinct change in the phenotype of glial filaments between 14-3-3γ knock down groups and control groups

The motile properties of GFAP in 14-3-3γ overexpressed glioma C6 cells was investigated by FRAP assay. When 14-3-3γ was overexpressed, the recovery of GFP-GFAP was slower compared with the control (Fig. 7B). The average half-time for GFP-GFAP filaments to recover fluorescence in the bleached zones ($t_{1/2}$) in the control untransfected glioma C6 cells was 217±30 seconds (n=20) (Fig. 7A,C). When DsRed-14-3-3γ was over-expressed, the recovery half-time of filamentous GFP-GFAP which was colocalized with DsRed-14-3-3γ, increased to 410±45 seconds (n=15) (Fig. 7B,C). In addition, the aggregation of GFP-GFAP dots colocalized with DsRed-14-3-3γ hardly recovered any fluorescence during the 30 minutes of observation after photobleaching (Fig. 7B,C). These results indicated that both the movement of GFP-GFAP dots and the formation of GFP-GFAP filaments were slowed down by the overexpression of 14-3-3γ.

Discussion

GFAP is a marker of astrocytes that polymerizes into 10 nm diameter filaments with vimentin (Abd-el-Basset et al., 1992). In general, a distinct intermediate filament network during interphase in vivo assembles and disassembles ceaselessly in a dynamic manner (Helfand et al., 2004). Our results showed that GFAP, vimentin and 14-3-3γ all exist in both detergent soluble and insoluble fractions, and coimmunoprecipitation also demonstrated that these proteins might interact with each other to form a physical complex (Fig. 1A,B). Immunostaining showing co-localization of cytoplasmic punctate GFAP with 14-3-3γ, supported this finding (Fig. 3Bd-f and Fig. 4Ca-c). The soluble GFAP and vimentin were derived from two sources. Some were newly synthesized in the cytoplasm, whereas others came from the disassembly of the glial filament network. Since 14-3-3γ was colocalized with filamentous GFAP in a few interphase (Fig. 4Ca-c) and most prophase astrocytes (Fig. 3Bg-i), it seemed that 14-3-3γ proteins could associate with filamentous GFAP under certain conditions or during special phases of the cell cycle. Thus results suggest that 14-3-3γ can bind to GFAP or the GFAP/vimentin complex in both non-filamentous and filamentous structures, with some 14-3-3γ proteins distributed freely in the cytoplasm.

In our research, using SW13 Cl1 vimentin (+) cell line, native 14-3-3γ can interact with vimentin in both soluble (non-filamentous) and insoluble (filamentous) fractions in the absence of GFAP (Fig. 1D), similar to the association of 14-3-3ζ and vimentin in cos7 cells (Tzivion et al., 2000). In SW13 Cl2 vimentin (–) cells, transfected GFAP can assemble to form 10 nm intermediate filaments (Fig. 4C), and the native 14-3-3γ can interact with both detergent soluble and insoluble fractions of exogenous GFAP. This means that the expression of vimentin has no influence on the association of GFAP and 14-3-3γ in vivo. Thus both GFAP and vimentin can associate
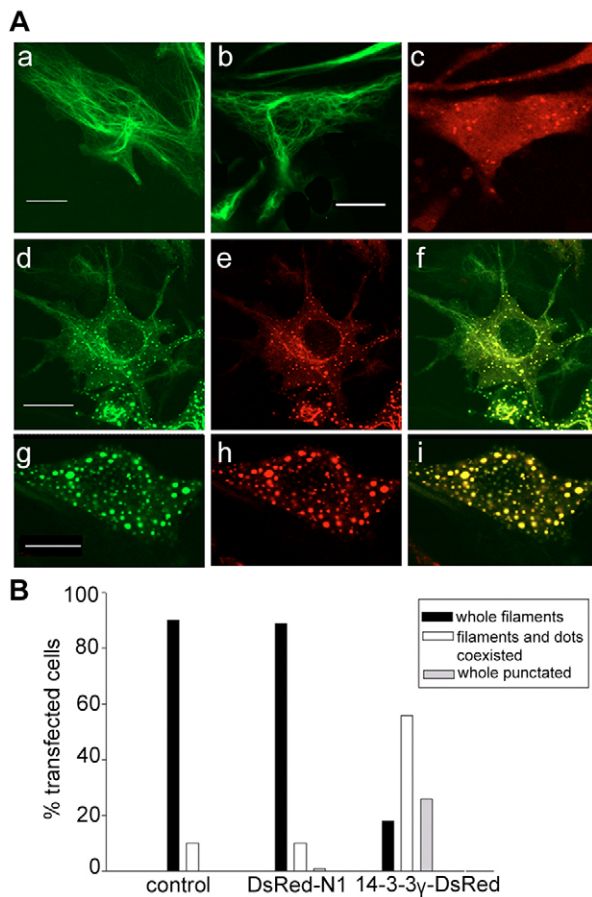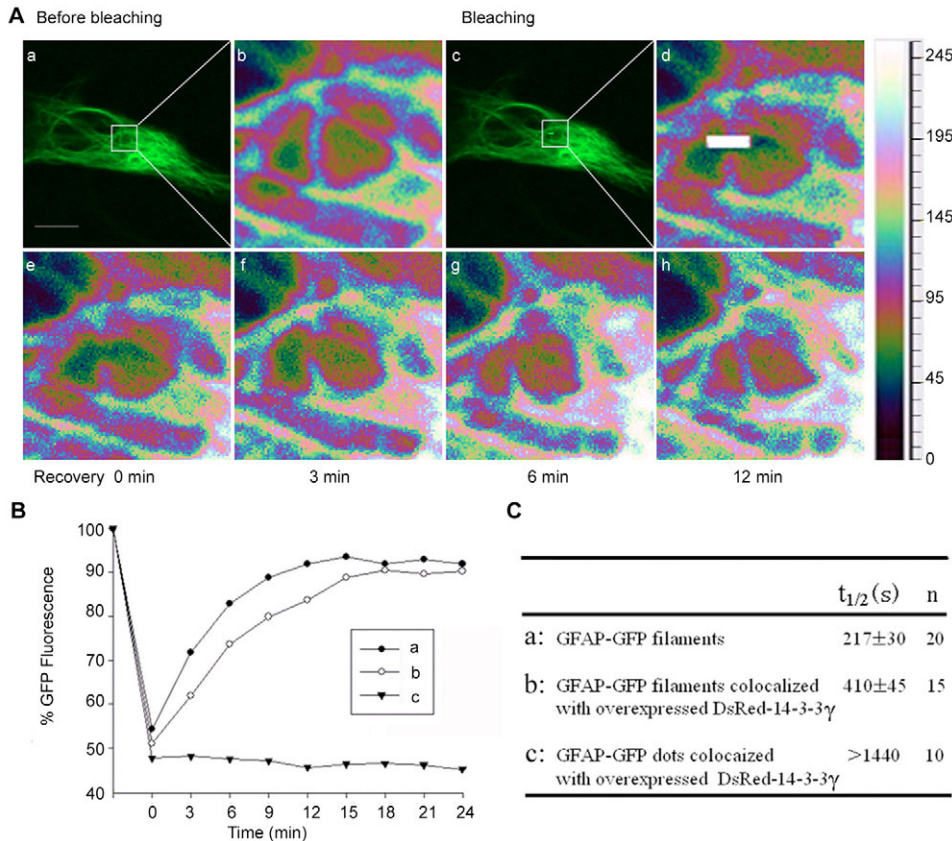
Fig. 7. Motile properties of GFAP in 14-3-3γ overexpressed glioma C6 cells. (A) Cells transfected with GFP-GFAP were imaged before (a,b), after bleaching (c,d), and during recovery (e-h). Images were taken at the indicated times after the end of the bleach pulse. The indicated area is enlarged in pseudocolour (b,d,e-h) and the fluorescence density is shown on the right. (B) Quantitative analysis of FRAP experiments after bleaching. Cells expressing only GFP-GFAP were detected as the control (a). Two different colocalized forms of GFAP, filaments (b) and dots (c), were both examined in GFP-GFAP and DsRed-14-3-3γ cotransfected cells. (C) The $t_{1/2}$ of FRAP in the above three groups were calculated. Scale bar, 10 μm. Scale bar in magnified figure, 1 μm.

with 14-3-3γ, and one association can occur independently of the other association. Though vimentin was detected in the GFAP-14-3-3γ physical complex in primary cultured astrocytes, vimentin did not play an essential role in the interaction of GFAP with 14-3-3γ. This is in contrast to the situation in simple-type epithelial cells in which both their keratin intermediate filament proteins, K8 and K18, are needed for 14-3-3ζ association (Ku et al., 1998).

The phosphorylation and dephosphorylation of IFs is closely related to the cell cycle. In interphase, the filamentous structure of GFAP is in a lower phosphorylation state, which then gradually increases during S to G2/M phases of the cell cycle. The level of phosphorylation depends on the activities of kinases and phosphatases in the cytoplasmic matrix (Yasui et al., 1998). During interphase, 14-3-3γ proteins were observed distributed freely or colocalized with dots of soluble GFAP, with little bound to GFAP filaments (Fig. 3Bd-f). Hyperphosphorylation of the IF proteins resulted in the disassembly of IF networks when cells entered mitosis in some cell types. During prophase, 14-3-3γ proteins were mainly bound to GFAP filaments that were about to disassemble (Fig. 3Bg-l). Therefore, 14-3-3γ proteins can associate with nonfilamentous GFAP in astrocytes during interphase, and bind to filamentous GFAP during the G2/M phase of the cell cycle. These results indicate that the cell cycle dependent association of 14-3-3γ with GFAP filaments and the subsequent filament disassembly is likely to be due to phosphorylation of GFAP by cell cycle-dependent kinases.

Although the role of 14-3-3 proteins in higher eukaryotes is not well understood, yeast 14-3-3 homologs play an important role in determining the timing of mitosis in *Schizosaccharomyces pombe* (Ford et al., 1994). Given the association of 14-3-3 proteins with important cellular kinases, such as PKC, cdc25 (Dougherty and Morrison, 2004), the possibility of intracellular signaling or regulatory roles for 14-3-3γ associated with GFAP become highly attractive. Cdc2 kinase has been identified as a key regulator of GFAP organization during mitosis and its activity is very important for GFAP to accomplish its reorganization (Matsuoka et al., 1992; Tsujimura et al., 1994; Yasui et al., 1998). The association of GFAP and 14-3-3γ obviously increased after cdc2 kinase or PKC treatment (Fig. 2B). Therefore, the regulation of intermediate filament assembly and disassembly through 14-3-3γ and GFAP filament interaction, may, at least in astrocytes, be dependent on such cell cycle factors and might be important in the regulation of mitotic events.

The results of domain mapping experiments showed that the N terminal head domain of GFAP is necessary for the colocalization of 14-3-3γ and filamentous GFAP, and it predicts that the binding site of 14-3-3γ is located in the head domain. Furthermore, immunofluorescence and coimmunoprecipitation experiments showed that the S8A mutation in GFAP specifically blocks the binding of 14-3-3γ, indicating that phosphorylated GFAP serine 8 plays an essential role in the interaction between 14-3-3γ and GFAP. Ser8 in GFAP is the target site of PKA, PKC and cdc2 (Yasui et al., 1998). Previous reports did not find any mutation of Ser8 in Alexander disease (Brenner et al., 2001), however, mice with

ablation of several phosphorylation sites in GFAP including Ser8 exhibited unstable GFAP filaments, particularly in the absence of vimentin (Takemura et al., 2002).

Although overexpression of 14-3-3γ affected the assembly and movement of glial filaments (Figs 6, 7) clearly, knockdown of 14-3-3γ by RNAi did not change the phenotype of glial filaments (supplementary material Fig. S3). Knockout mice studies obtained similar results (Steinacker et al., 2005). Though 14-3-3γ has been used as a marker protein in the diagnosis of CJD, there was no distinct phenotype detected in 14-3-3γ knockout mice. Since 14-3-3 ε, ζ and β isoforms have been identified to interact with GFAP in astrocytes (Satoh et al., 2004), we considered that other 14-3-3 isoforms may play compensatory roles.14-3-3η didn't show interaction with GFAP in astrocytes (supplementary material Fig. S1), thus we considered that the target protein of different 14-3-3 isoforms showed a relative specificity.

Two high-affinity phosphorylation-dependent binding motifs are recognized by all 14-3-3 isotypes: RSXpSXP and RXXXpSXP (Dougherty and Morrison, 2004; Rittinger et al., 1999; Yaffe and Elia, 2001), where pS represents phosphoserine. However, phosphorylation-dependent sites that diverge significantly from these motifs have also been described (Aitken, 2002). The keratin, K18-Ser33-containing motif (RPVSSAApSVY) is also different from these two conserved motifs (Ku et al., 1998). Interestingly, the GFAP-Ser8-containing motif (RRITpSAR) appears to be very different from these conserved motifs, suggesting that RRITpSAR is a newly identified 14-3-3 binding motif.

Our data unambiguously show that first, 14-3-3γ interacts directly with GFAP independently of vimentin in astrocytes; second, this interaction is dependent on GFAP phosphorylation and serine 8 in mus GFAP head domain is essential for 14-3-3γ binding. We propose a model in which the subunits of GFAP filaments in astrocytes are phosphorylated during prophase of the cell cycle, allowing 14-3-3γ binding to phosphorylated serine 8 of GFAP head domain. This would regulate the disassembly of the GFAP intermediate filaments. This work illustrates a role for 14-3-3 proteins in IF dynamics in the nervous system. Understanding this process may help unravel fundamental aspects of cytoskeleton assembly and some mechanisms of CNS neurodegeneration.

Materials and Methods

cDNA construction
The mouse GFAP cDNA was synthesized by RT-PCR (primer 1: GGATCCATGGGAGCGGAGACGC, primer 2: AATTCCCATCACCACGTCCTTG) using an mRNA sample extracted from a mouse brain. The cDNA of 14-3-3γ was cloned from a mouse cDNA library by means of differential display under ischemia (Chen et al., 2003). GFAP deletion mutants, ΔH (Δ4-207), ΔT (Δ1123-1289) and phosphorylation site mutants (S8A, S12A, S15A and S35A) were constructed by PCR amplification of the corresponding cDNA fragments. The GFAP cDNA and its mutants were subcloned into BglII/EcoRI sites on pEGFP-N1 or pEYFP-N1 vectors (CLONTECH Laboratories, Inc.), and into BamHI/EcoRI sites on pCMV5C vector (Stratagene Corp.). The cDNA of GFAP was also inserted into BamHI and EcoRI sites on pcDNA3.1 (+) vector (Invitrogen Corp.). 14-3-3γ cDNA was inserted into BamHI/EcoRI on pDsRed-N1 and pECFP-N1 vectors (CLONTECH Laboratories).

Cell culture and transfection
Primary astrocytes were prepared from 1-day-old ICR mice. Following anaesthesia and decapitation, brains were removed aseptically and placed in sterile culture dishes containing Dulbecco's Modified Eagle Medium (DMEM) (GIBCO BRL, Gaithersburg, MD). Meninges, midbrain and vessels were removed. The tissue was minced with scissors and incubated with 1 ml 0.25% trypsin at 37°C for 15 minutes. The cell suspension was then subsequently passed through sterile nylon filters with a pore size of 70 μm and 50 μm to remove remnants of blood vessels and meninges. Cell suspension was diluted with DMEM supplemented with 10% fetal bovine serum (FBS) and transferred to 35 mm dishes (8 dishes per brain). They were incubated at 37°C in 5% CO_2. The media was replaced twice weekly with DMEM supplemented with 10% FBS. Rat glioma C6, human adrenal carcinoma SW13 Cl1 (Vim+) and SW13 Cl2 (Vim-) cell lines (kind gifts from Dr Robert M. Evans, University of Colorado Health Sciences Center, Denver, CO) (Sarria et al., 1990) were grown in DMEM containing 10% FBS at 37°C in 5% CO_2. Transient transfection was performed with Lipofectamine™2000 reagent (Invitrogen Corp.) in cultures at ~80% confluency. Transfected cells were allowed to grow for an additional 36-48 hours before further experiments.

Small interfering RNA studies
We designed siRNA to interfere with the expression of rat 14-3-3γ mRNA, according to the supplier's technical information (Ambion, Austin, TX). The annealed insert was cloned into the pSilencer 2.1-U6 neo vector, digested with BamHI and HindIII. Transient transfection of interfering plasmid into C6 cells was performed and the effects of siRNAs were examined 48 h after transfection. The pSilencer 2.1-U6 neo vector was used as negative control.

Calyculin A, CIAP and kinase treatment
For inhibition of type 1 (PP1) and type 2A (PP2A) serine/threonine phosphatases, cells were treated with 100 nM Calyculin A (Cl-A, Sigma Chemical) for 1 hour and then harvested. In dephosphorylation experiments, cell lysates were treated with 20 unit ml^{-1} calf intestinal alkaline phosphatase (CIAP, Promega Corp.) at 30°C for 30 minutes before use. In the kinase assay, immunoisolated complex were treated with cdc2 kinase (Promega Corp.) or Protein Kinase C (PKC, Promega Corp.) for 30 minutes at 30°C in their respective buffers (detailed in Promega product description).

Cell synchronization
Some astrocytes were synchronized in primary culture of 60% confluence at G1/S phase by 24 hours treatment of 5 μg ml^{-1} DNA polymerase-α inhibitor, aphidicolin. Cells were rinsed with serum-free culture medium to remove traces of the drug, and incubated in 10% FBS containing culture medium for 5-6 hours (S phase enriched), or 10-12 hours (G2/M phase enriched) (Liao and Omary, 1996).

Immunoblot analysis
Samples were prepared by adding SDS-PAGE loading buffer to the culture after washing with PBS. After gel electrophoresis, the proteins were transferred onto Magna Nitrocellulose Supported Transfer Membrane (Osmonics) and probed with primary antibodies at 37°C for 2 hours. Alkaline phosphatase conjugated goat anti-mouse and goat anti-rabbit IgG antibodies (Cappel Laboratories, Cochranville, PA) were used as secondary antibodies. The results were revealed by the NBT-BCIP (Promega Corp.) reaction. Primary antibodies used were: mouse anti-GFAP monoclonal antibody, 1:200 (Sigma Chemical Corp.), rabbit anti-GFAP polyclonal antibody, 1:500 (Eng and DeArmond, 1983), mouse anti-vimentin monoclonal antibody, 1:100 (Santa Cruz, Calif.), mouse anti-c-myc (9E10) monoclonal antibody, 1:200 (Santa Cruz, CA), goat anti-14-3-3η polyclonal antibody, 1:200 (Santa Cruz, CA), mouse anti-14-3-3γ monoclonal antibody, 1:1000 (Upstate, Charlottesville) and rabbit anti-14-3-3γ polyclonal antibody, 1:100 (Santa Cruz, CA).

Immunofluorescence
Cells grown on coverslips pretreated with 12.5 μg ml^{-1} poly-L-lysine (Sigma Chemical Corp.) were washed in cold PBS, fixed with 4% paraformaldehyde in PBS for 20 minutes and permeabilized with 0.2% Triton X-100 in PBS for 10 minutes at room temperature. After blocking with 1% BSA in PBS for at least 15 minutes, the cells were incubated with primary antibodies for 2 hours at 37°C. The secondary antibodies were FITC-conjugated goat anti-mouse IgG and/or rhodamine-conjugated goat anti-rabbit IgG. Triple staining was done using two primary antibodies and 1 μg/ml Hoechst 33342 (Molecular Probes, OR) for nuclear staining. Samples were observed with the TCS SP2 confocal microscope (Leica, Germany).

Immunoprecipitation
Cells were washed three times with PBS and lysed in lysis buffer (20 mM Tris-HCl [pH: 8.0], 10% glycerol, 5 mM MgCl2, 0.5% NP-40, 25 μg/ml aprotinin, 150 mM KCl, 50 mM NaF). The lysates were centrifuged at 12,000 g for 30 minutes. The supernatants were mixed with 15 μl rabbit preimmune serum or rabbit antibody and incubated at 4°C for 3 hours. Then 20 μl protein A-Sepharose beads (Pharmacia) were added and the mixtures were rotated overnight at 4°C. After washing extensively with lysis buffer, the bound immunocomplexes were eluted by boiling in SDS sample buffer and subjected to western blot analysis. The post-NP-40 pellet was washed with lysis buffer and boiled in SDS sample buffer for western blot.

Fluorescence resonance energy transfer (FRET)
To detect direct interaction between two proteins in a single cell, an acceptor photobleaching method was used to measure FRET (Kotevic et al., 2005).

Transfected cells were fixed in 4% paraformaldehyde for 20 minutes before measurement. Cyan fluorescence protein (CFP)-linked fusion protein (donor) was excited at 458 nm and fluorescence emission was detected using a 470–500 nm bandpass filter. Yellow fluorescence protein (YFP)-linked fusion protein (acceptor) was excited at 514 nm and fluorescence emission was detected using a 526-600 nm bandpass filter. Donor and acceptor fluorescence before and after bleaching of YFP was recorded. In each cell, a single region of interest (ROI 1) was bleached using the 514 nm laser at maximum intensity. The time for bleaching ranged between 5 and 10 frames depending on the size of ROI 1. CFP and YFP images were collected before and after the bleaching step to control for stability of the fluorescence signal. The change in FRET efficiency as the percentage of total donor fluorescence in the absence of the acceptor (Ef) was calculated by Leica FRET software. Similar calculations were performed in a non-bleached region (ROI 2) of the image to obtain the parameter control efficiency (Cf) representing an internal control value that under ideal conditions should be zero. About 20 cells were measured for each slide. YFP-tagged GFAP domain deletion mutants and CFP-tagged 14-3-3γ were co-transfected into SW13 Cl2 cells to detect direct interactions between 14-3-3γ and GFAP deletion mutants.

Fluorescence recovery after photobleaching (FRAP)

C6 cells were transfected with pEGFP-GFAP and pDsRed-14-3-3γ simultaneously or with pEGFP-GFAP alone, to detect the movements of EGFP-GFAP filaments and dots using FRAP. Phase-contrast images of cells were taken before and immediately after FRAP to ensure that there were no significant changes in cell shape or position. Bar-shaped regions were bleached using the line-scan function at 488 nm (100% power), and recovery of fluorescence was monitored (10% power) using the time-series function at 3 minute intervals for up to 30 minutes. Fluorescence recovery was analyzed using Leica software, and $t_{1/2}$ was calculated as the time needed to reach half of the original intensity after photobleaching. Unbleached regions were used as controls. 10-20 cells were measured in each sample and the average $t_{1/2}$ was calculated.

References

Abd-el-Basset, E. M., Ahmed, I., Kalnins, V. I. and Fedoroff, S. (1992). Immuno-electron microscopical localization of vimentin and glial fibrillary acidic protein in mouse astrocytes and their precursor cells in culture. *Glia* **6**, 149-153.

Aitken, A. (2002). Functional specificity in 14-3-3 isoform interactions through dimer formation and phosphorylation. Chromosome location of mammalian isoforms and variants. *Plant Mol. Biol.* **50**, 993-1010.

Brenner, M., Johnson, A. B., Boespflug-Tanguy, O., Rodriguez, D., Goldman, J. E. and Messing, A. (2001). Mutations in GFAP, encoding glial fibrillary acidic protein, are associated with Alexander disease. *Nat. Genet.* **27**, 117-120.

Chen, W. J. and Liem, R. K. (1994). The endless story of the glial fibrillary acidic protein. *J. Cell Sci.* **107**, 2299-2311.

Chen, X. Q., Chen, J. G., Zhang, Y., Hsiao, W. W. and Yu, A. C. (2003). 14-3-3gamma is upregulated by in vitro ischemia and binds to protein kinase Raf in primary cultures of astrocytes. *Glia* **42**, 315-324.

Dougherty, M. K. and Morrison, D. K. (2004). Unlocking the code of 14-3-3. *J. Cell Sci.* **117**, 1875-1884.

Eng, L. F. and DeArmond, S. J. (1983). Immunochemistry of the glial fibrillary acidic protein. *Prog. Neurobiol.* **5**, 19-39.

Ford, J. C., al-Khodairy, F., Fotou, E., Sheldrick, K. S., Griffiths, D. J. and Carr, A. M. (1994). 14-3-3 protein homologs required for the DNA damage checkpoint in fission yeast. *Science* **265**, 533-535.

Fountoulakis, M., Cairns, N. and Lubec, G. (1999). Increased levels of 14-3-3 gamma and epsilon proteins in brain of patients with Alzheimer's disease and Down syndrome. *J. Neural Transm. Suppl.* **57**, 323-335.

Fu, H., Subramanian, R. R. and Masters, S. C. (2000). 14-3-3 proteins: structure, function, and regulation. *Annu. Rev. Pharmacol. Toxicol.* **40**, 617-647.

Helfand, B. T., Chang, L. and Goldman, R. D. (2004). Intermediate filaments are dynamic and motile elements of cellular architecture. *J. Cell Sci.* **117**, 133-141.

Hermeking, H. (2003). The 14-3-3 cancer connection. *Nat. Rev. Cancer* **3**, 931-943.

Kawajiri, A., Yasui, Y., Goto, H., Tatsuka, M., Takahashi, M., Nagata, K. and Inagaki, M. (2003). Functional significance of the specific sites phosphorylated in

desmin at cleavage furrow: Aurora-B may phosphorylate and regulate type III intermediate filaments during cytokinesis coordinately with Rho-kinase. *Mol. Biol. Cell* **14**, 1489-1500.

Kotevic, I., Kirschner, K. M., Porzig, H. and Baltensperger, K. (2005). Constitutive interaction of the P2Y2 receptor with the hematopoietic cell-specific G protein G(alpha16) and evidence for receptor oligomers. *Cell. Signal.* **17**, 869-880.

Ku, N. O., Liao, J. and Omary, M. B. (1998). Phosphorylation of human keratin 18 serine 33 regulates binding to 14-3-3 proteins. *EMBO J.* **17**, 1892-1906.

Ku, N. O., Michie, S., Resurreccion, E. Z., Broome, R. L. and Omary, M. B. (2002). Keratin binding to 14-3-3 proteins modulates keratin filaments and hepatocyte mitotic progression. *Proc. Natl. Acad. Sci. USA* **99**, 4373-4378.

Liao, J. and Omary, M. B. (1996). 14-3-3 proteins associate with phosphorylated simple epithelial keratins during cell cycle progression and act as a solubility cofactor. *J. Cell Biol.* **133**, 345-357.

Liedtke, W., Edelmann, W., Bieri, P. L., Chiu, F. C., Cowan, N. J., Kucherlapati, R. and Raine, C. S. (1996). GFAP is necessary for the integrity of CNS white matter architecture and long-term maintenance of myelination. *Neuron* **17**, 607-615.

Magin, T. M., Reichelt, J. and Hatzfeld, M. (2004). Emerging functions: diseases and animal models reshape our view of the cytoskeleton. *Exp. Cell Res.* **301**, 91-102.

Matsuoka, Y., Nishizawa, K., Yano, T., Shibata, M., Ando, S., Takahashi, T. and Inagaki, M. (1992). Two different protein kinases act on a different time schedule as glial filament kinases during mitosis. *EMBO J.* **11**, 2895-2902.

Moore, B. W. and Perez, V. J. (1967). Specific acidic proteins of the nervous system. In *Physiological and Biochemical Aspects of Nervous Integration* (ed. F. D. Carlson), pp. 343-369. Englewood Cliffs, NJ: Prentice-Hall.

Pekny, M. and Nilsson, M. (2005). Astrocyte activation and reactive gliosis. *Glia* **50**, 427-434.

Rittinger, K., Budman, J., Xu, J., Volinia, S., Cantley, L. C., Smerdon, S. J., Gamblin, S. J. and Yaffe, M. B. (1999). Structural analysis of 14-3-3 phosphopeptide complexes identifies a dual role for the nuclear export signal of 14-3-3 in ligand binding. *Mol. Cell* **4**, 153-166.

Sarria, A. J., Nordeen, S. K. and Evans, R. M. (1990). Regulated expression of vimentin cDNA in cells in the presence and absence of a preexisting vimentin filament network. *J. Cell Biol.* **111**, 553-565.

Satoh, J., Yamamura, T. and Arima, K. (2004). The 14-3-3 protein epsilon isoform expressed in reactive astrocytes in demyelinating lesions of multiple sclerosis binds to vimentin and glial fibrillary acidic protein in cultured human astrocytes. *Am. J. Pathol.* **165**, 577-592.

Sekimata, M., Tsujimura, K., Tanaka, J., Takeuchi, Y., Inagaki, N. and Inagaki, M. (1996). Detection of protein kinase activity specifically activated at metaphase-anaphase transition. *J. Cell Biol.* **132**, 635-641.

Steinacker, P., Schwarz, P., Reim, K., Brechlin, P., Jahn, O., Kratzin, H., Aitken, A., Wiltfang, J., Aguzzi, A., Bahn, E. et al. (2005). Unchanged survival rates of 14-3-3gamma knockout mice after inoculation with pathological prion protein. *Mol. Cell. Biol.* **25**, 1339-1346.

Takemura, M., Gomi, H., Colucci-Guyon, E. and Itohara, S. (2002). Protective role of phosphorylation in turnover of glial fibrillary acidic protein in mice. *J. Neurosci.* **22**, 6972-6979.

Tsujimura, K., Tanaka, J., Ando, S., Matsuoka, Y., Kusubata, M., Sugiura, H., Yamauchi, T. and Inagaki, M. (1994). Identification of phosphorylation sites on glial fibrillary acidic protein for cdc2 kinase and Ca(2+)-calmodulin-dependent protein kinase II. *J. Biochem.* **116**, 426-434.

Tzivion, G., Luo, Z. J. and Avruch, J. (2000). Calyculin A-induced vimentin phosphorylation sequesters 14-3-3 and displaces other 14-3-3 partners in vivo. *J. Biol. Chem.* **275**, 29772-29778.

Van Everbroeck, B. R., Boons, J. and Cras, P. (2005). 14-3-3{gamma}-isoform detection distinguishes sporadic Creutzfeldt-Jakob disease from other dementias. *J. Neurol. Neurosurg. Psychiatr.* **76**, 100-102.

Watanabe, M., Isobe, T., Ichimura, T., Kuwano, R., Takahashi, Y. and Kondo, H. (1993). Molecular cloning of rat cDNAs for beta and gamma subtypes of 14-3-3 protein and developmental changes in expression of their mRNAs in the nervous system. *Brain Res. Mol. Brain Res.* **17**, 135-146.

Weinstein, D. E., Shelanski, M. L. and Liem, R. K. (1991). Suppression by antisense mRNA demonstrates a requirement for the glial fibrillary acidic protein in the formation of stable astrocytic processes in response to neurons. *J. Cell Biol.* **112**, 1205-1213.

Wilhelmsson, U., Li, L., Pekna, M., Berthold, C. H., Blom, S., Eliasson, C., Renner, O., Bushong, E., Ellisman, M., Morgan, T. E. et al. (2004). Absence of glial fibrillary acidic protein and vimentin prevents hypertrophy of astrocytic processes and improves post-traumatic regeneration. *J. Neurosci.* **24**, 5016-5021.

Yaffe, M. B. and Elia, A. E. (2001). Phosphoserine/threonine-binding domains. *Curr. Opin. Cell Biol.* **13**, 131-138.

Yasui, Y., Amano, M., Nagata, K., Inagaki, N., Nakamura, H., Saya, H., Kaibuchi, K. and Inagaki, M. (1998). Roles of Rho-associated kinase in cytokinesis; mutations in Rho-associated kinase phosphorylation sites impair cytokinetic segregation of glial filaments. *J. Cell Biol.* **143**, 1249-1258.